Investigating the impact of neutrons on Cadmium Zinc Telluride Compton camera

J De Klerk, A Buffler, T Hutton and S Peterson

Department of Physics, University of Cape Town, Rondebosch 7700, South Africa

E-mail: josiahchristiandeklerk@gmail.com

Abstract. During proton therapy (PT), excited-nuclei decay via emission of characteristic prompt gamma rays along the beam path within the target. These gamma rays are detectable via a Compton camera and can be used for in vivo proton beam range verification using a technique called prompt gamma imaging (PGI). The detection efficiency of a PGI device can be negatively affected by additional secondary radiation (primarily neutrons). The UCT Prompt gamma imaging system (Polaris) is a room temperature solid state Compton camera detector. The imaging device comprises of two independent detection platforms with each consisting of two Cadmium Zinc Telluride crystals (20 x 20 x 10 mm^3) arranged side-by-side. The goal of the project is to better understand the impact of neutrons on the Polaris detectors during PT and compare its response to NaI and $LaBr_3$ and NE213. These more traditional detectors act as means of calibration for expected gamma ray spectra in the Polaris detectors and to highlight any impact of neutrons on the Cadmium Zinc Telluride crystals. Preliminary results are presented from measurements conducted at the UCT n-lab MeASURe facility (neutrons up to 14 MeV) and at iThemba LABS (66 MeV proton beam).

1. Introduction

1.1. Proton therapy

Proton therapy, a form of radiation therapy, has been used effectively in cancer and tumour treatment [1]. The benefits of PT lie fundamentally in how incident protons interact inside tissue. As protons transverse through tissue, energy is transferred to the surrounding electrons via coulomb interactions. Most of the proton energy is transferred toward the end of its trajectory where maximum ionisation loss takes place known as the Bragg peak [2]. After the Bragg peak, the rate of ionisation slows down to a point where there is no more energy being transferred and the protons path comes to an end [3]. It can be said that the proton beam has a finite range. The characteristics of the Bragg peak and finite range found in PT allows it to produce high conformal treatment [4], prevent large exposure to healthy tissue and reduce treatment side effects (acute and late) [5].

1.2. Compton camera (CC)

The inelastic interaction of interest during PT is prompt emission. Excited nuclei decay via emission of a characteristic prompt gamma (PG) ray. Since nuclei are quantized, the PG ray energies are specific to the excited nuclei and hence specific to the material type. Furthermore, PGs are produced during treatment at the dose location within a few nanosecond, making them suitable for beam verification [6]. One way PGs are detected is by a device known as a Compton

camera (CC). A traditional CC consists of at least two detectors, one acting as a scatterer and the other as an absorber, that operate coincidentally (figure 1). The key interactions for Compton imaging are Compton scattering and photoelectric absorption. PGs incident to a CC scatter at an angle θ, undergoing a Compton interaction where some energy is transferred to an electron, referred to as the recoil electron. Here, the energy and position of the PG is recorded. The above can be described by the following relationship of the incident PG energy E_0, the deposited energy E_1 and the angle of scatter θ_1 [7]:

$$cos(\theta_1) = 1 + m_e c^2 (\frac{1}{E_0} - \frac{1}{E_0 - E_1}) \tag{1}$$

The last detector absorbs the scattered PG by means of photoelectric absorption.

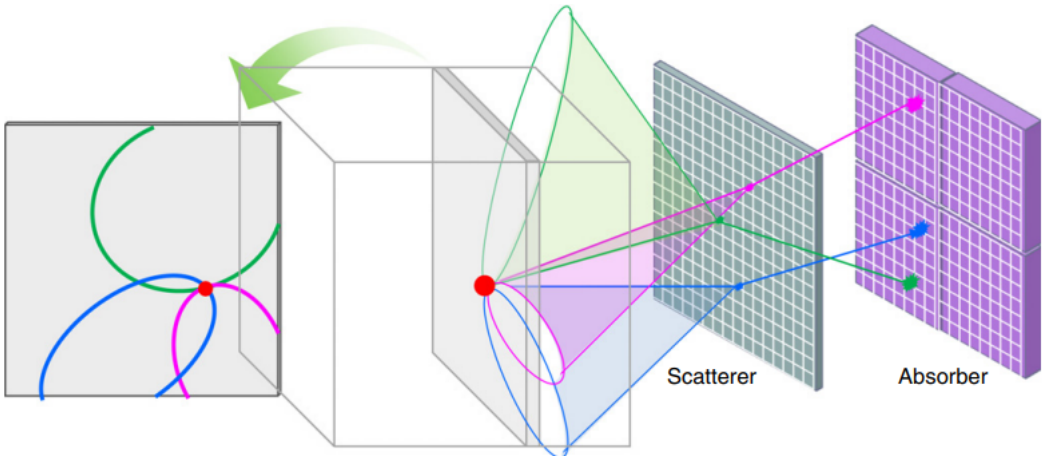

Figure 1. An example of a traditional Compton camera with a scatterer and an absorber. The image displays several prompt gammas being projected onto their respective cones.[8]

The combination of at least two interactions enables the calculation of the incident PG energy and the construction of a cone of origin. The emission point of a PG is restricted onto the surface of a constructed cone with the intersection of several cones resulting in an image of the source location [8] (figure 1). Methods of image reconstruction include back projections and statistical means [9]. CCs have been used as a means for in vivo proton beam range verification of a patient through PG imaging for clinical use [10]. For a PG imaging (PGI) system to be viable for clinical use, the system needs to have sufficient statistics, good position and energy resolution and the capability to manage the count rate ranges of PGs [11]. Moreover, other PGI factors include detector positioning sensitivity, statistical uncertainties and contamination from secondary neutrons [12]. In a study conducted at the University of Maryland School of Medicine, the results for a Cadmium Zinc Telluride (CZT) PGI system system have successfully produced three-dimensional images. However, these results were limited by detection rates due to secondary radiation during PT [9]. Furthermore, work done by [13] reports the degrading of image quality by secondary neutron induced PG. These PG are a result of the secondary neutrons produced inside the body interacting with tissue and undergoing prompt emission. Secondary neutrons are not only produced internally [14] but also externally from the proton treatment nozzle [15]. CZT CCs easily detect thermal neutrons over fast neutrons due to the high interactions cross section of neutron capture [16]. However, the secondary neutrons emitted from PT are predominantly fast neutrons. At these high neutron energies, the probability that a neutron will interact through neutron capture reduces and interactions through inelastic or elastic scattering dominate.

1.3. UCT PGI system

The UCT PGI system (Polaris) is a room temperature solid-state detector built by H3D Inc. [Ann Arbor, MI USA]. The CC consists of two independent Polaris detection platforms (figure 2). Each platform consists of two CZT crystals (20 x 20 x 10 mm) arranged side-by-side,

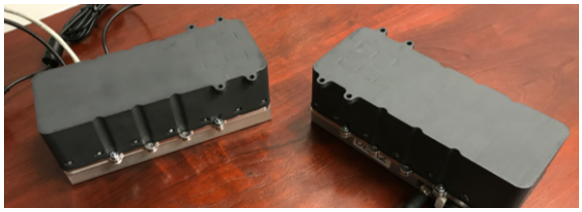

Figure 2. UCT Polaris detectors

a total of four crystals. The crystals are pixilated 11 x 11 in the x and y directions with depth of interaction in the z-direction. The aforementioned features provides position-sensitive gamma detection in three-dimensions, an energy resolution of 0.8% FWHM at 662 keV [17] and its compact size is practically suited to be alongside patients during PT. Particles detected by Polaris are not distinguishable on an event-by-event basis. This adds to the problem of distinguishing between PGs emitted from proton-nucleus and neutron-nucleus interactions and other secondary particles produced during PT (such as neutrons). A starting point to solve the problem at hand is to characterise the capability of Polaris through exposure to both neutrons and gamma particles/fields. As a result, a series of measurements have been conducted at the UCT MeASURe facility and at iThemba labs making use of several detectors in conjunction with Polaris.

2. Measurements

2.1. UCT MeASURe facility

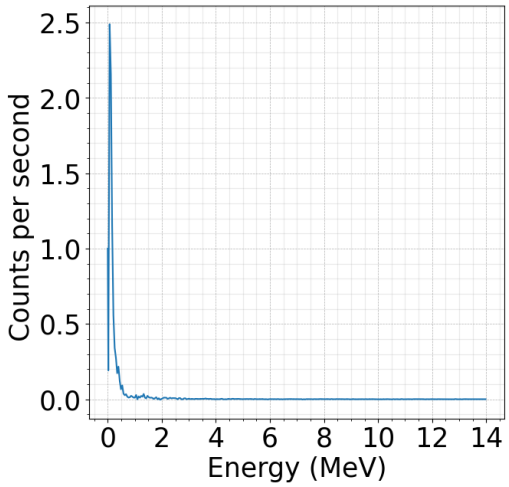

Figure 3. Polaris exposed to 14 MeV STNG neutrons incident on H_2O.

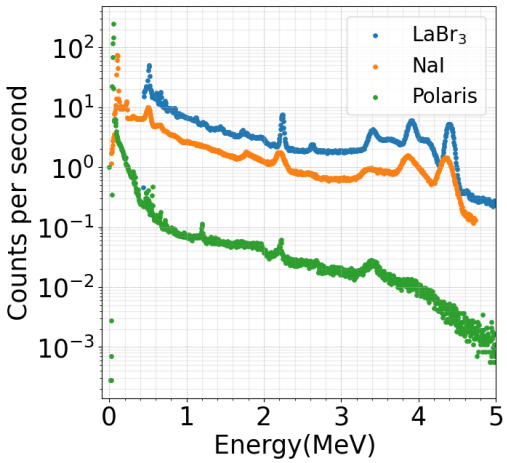

Figure 4. 4.4 AmBe gamma comparison

In graph 3, a normalised background removed gamma spectrum of deuterium-tritium sealed tube (STNG) incident to a block of water can be seen. The STNG produces monoenergetic neutrons with energy of 14 MeV. A 2.2 MeV gamma ray is also produced from neutron capture on the hydrogen is produced. This is not observed, potentially due to low count rates. As mentioned

previously, CZT is sensitive to thermal neutrons due to the high interaction cross-section of Cd but can not directly detect fast neutrons. Fast neutrons can be inferred by the recording of the recoil nuclei. These energies are low due to the small mass of neutrons relative to that of CZT. Unfortunately, the energy threshold of the Polaris detectors are not low enough for these recoil energies to be recorded.

NaI and $LaBr_3$ have been used as a source of comparison for an Americium-Beryllium (AmBe) source placed inside a block of High Density Polyethylene. The AmBe source produces neutrons over a broad energy spectrum from 0 to around 11 MeV and a 4.4 MeV gamma ray from the de-excitation of ^{12}C. The peaks of interest are 2.2 MeV gamma ray from neutron capture on hydrogen, 3.4 MeV single escape peak, 3.9 MeV double escape peak and 4.4 MeV gamma ray from the de-excitation of ^{12}C. From figure 4, no prominent peaks for both 3.9 MeV and 4.4 MeV is observed in the Polaris spectrum.

2.2. iThemba labs measurements

Measurements were made using a 66 MeV pulsed proton beam at iThemba Labs inside the K600 vault. The targets used in these measurements were a water phantom, carbon and HDPE blocks with several configurations and several detectors including Polaris, NE213 (liquid organic scintillator) and three $LaBr_3$ detectors. Unfortunately a few days before the scheduled measurement time, the second Polaris detector stopped working. Figure 5 displays a configuration of a water phantom with NE213 at 0°, Polaris at 90° and $LaBr_3$ at 135°, 270° and 315° respectively. After each measurement run, the detectors were changed to encompass a variety of angles for each target respectively.

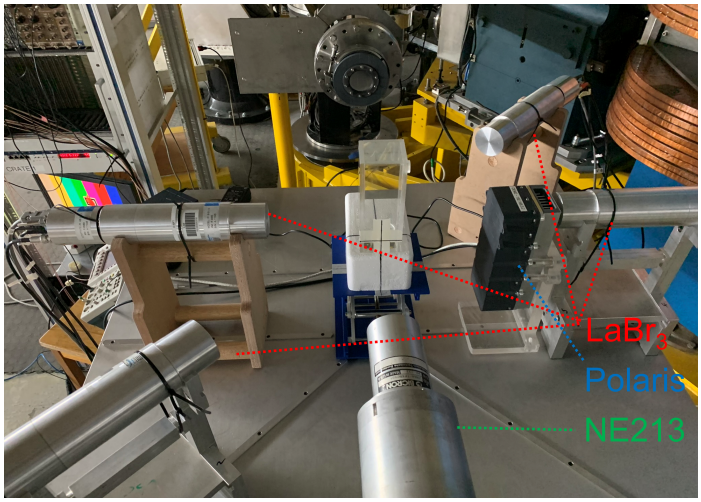

Figure 5. Detector configuration of 66 MeV proton incident on a water phantom.

From figure 6, count rates of Polaris begin to fall off at higher energies. An interesting aspect to note is that at 0° is where the highest count rates are observed. The same is not true for the pulse height(PH) spectrum from NE213 where a prominent peak is found at around 350°. It is speculated that this peak may be due to scattered protons from the beam window. The peak of interested is not seen at 0° and 270°, potentially due to the detector being shielded by the sample (0°) and/or the surface area of NE213 being exposed to scattered protons (270°). A further case for this is displayed in figure 7 with a high density line along the same channel number.

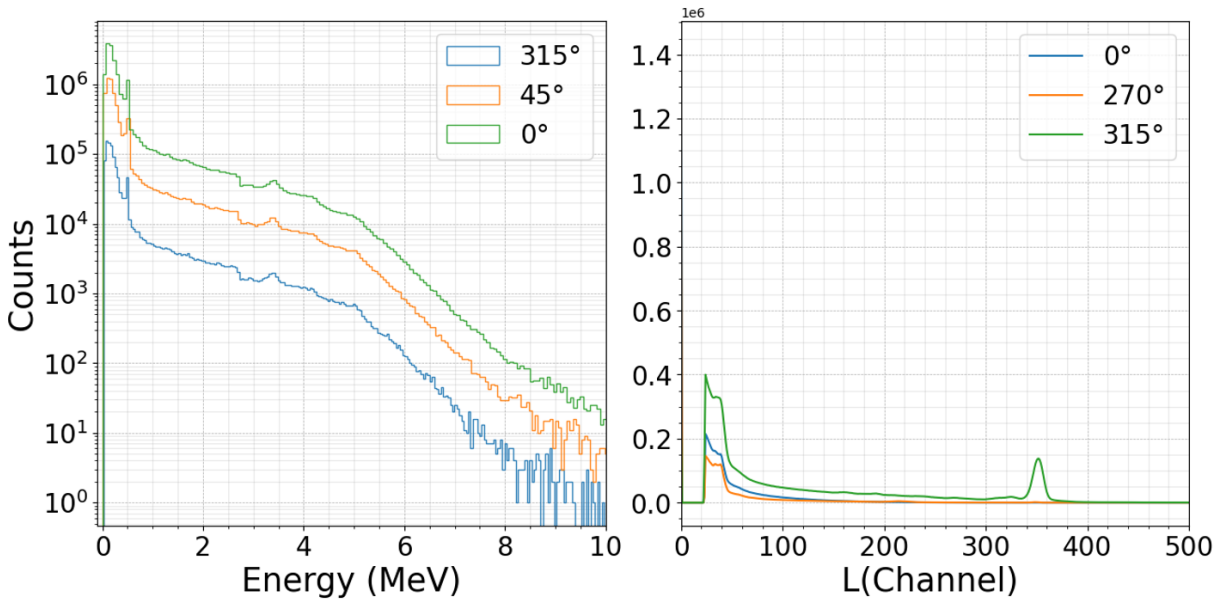

Figure 6. Left : Energy spectrum of water target from Polaris at various angles. Right : Pulse Height spectrum of water target from NE213 at various angles.

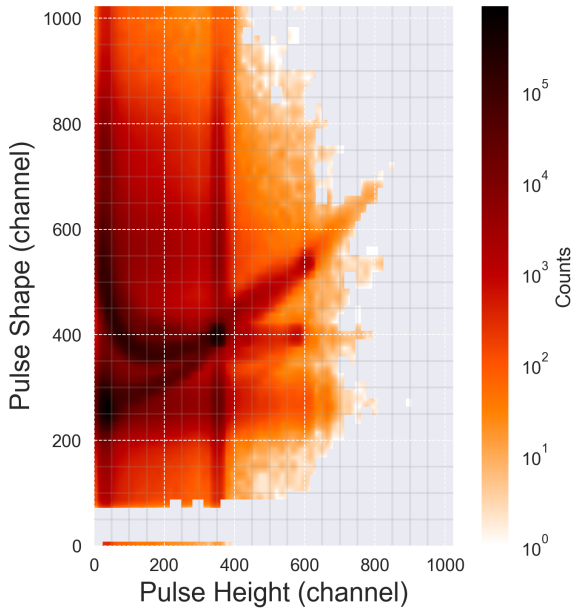

Figure 7. 2D pulse height and pulse shape of water at 315°.

3. Future work

The next step in the project involves producing energy spectrum (neutron and gamma) from the NE213 detector to be compared to Polaris. In order to obtain spectrum from NE213 one needs to employ a technique called unfolding. Unfolding requires both the PH spectrum of interest and a response matrix for both gammas and neutrons. The responses functions that make up the response matrices will be obtained from previous measurements taken in the d-line at iThemba

labs for neutrons and response functions for gammas will be calculated. The PH spectrum of gammas and neutrons are obtainable by Pulse shape(height) cuts that separate gammas and neutrons recorded by the detector. The goal is to discriminate good prompt gammas from the secondary radiation(neutrons).

4. Conclusion

Progress toward characterising Polaris has been made. Further analysis of neutron data will provide insights about the future developments of the Polaris system to be able to finally produce a viable clinical PGI system.

References

[1] Bertolet A and Carabe-Fernandez A 2020 Clinical implications of variable relative biological effectiveness in proton therapy for prostate cancer *Acta Oncol.* **59.10** 1171-1177

[2] Leo R W 1994 *Techniques for Nuclear and Particle Physics Experiments* Springer-Verlag Berlin Heidelberg New York p 28

[3] Martin R B and Shaw G 2019 *Nuclear and particle physics an introduction* John Wiley and Sons Ltd. p 156

[4] Mackin D, Peterson S, Beddar S and Polf J 2012 Evaluation of a stochastic reconstruction algorithm for use in Compton camera imaging and beam range verification from secondary gamma emission during proton therapy *Phys. Med. Biol* **57.11** 3537.

[5] Schneider U, Agosteo S, Pedroni E and Besserer J 2002 Secondary neutron dose during proton therapy using spot scanning *Rad. Oncol. Bio. Phys.* **53.1** 244-251.

[6] Polf J, Peterson S, McCleskey M, Roeder B, Spiridon A, Beddar S and Trache L 2009 Measurement and calculation of characteristic prompt gamma ray spectra emitted during proton irradiation *Phys. Med. Biol* **54.22** N519–27.

[7] Draeger E, Peterson S, Mackin D, Chen H, Beddar S, Polf J 2017 Feasibility studies of a new event selection method to improve spatial resolution of Compton imaging for medical applications *IEEE transactions on radiation and plasma medical sciences* **1.4** 358–367

[8] Kim S, Seo H, Park J, Kim C, Lee C, Lee S, Lee D, Lee J 2013 Resolution recovery reconstruction for a Compton camera *Phys. Med. Biol* **58.9** 2823.

[9] Draeger E, Mackin D, Peterson S, Chen H, Avery S, Beddar S and Polf J 2018 3D prompt gamma imaging for proton beam range verification *Phys. Med. Biol* **63.3** 035019.

[10] Maggi P, Peterson S, Panthi R, Mackin D, Yang H, He Z, Beddar S and Polf J 2020 Computational model for detector timing effects in Compton-camera based prompt-gamma imaging for proton radiotherapy *Phys. Med. Biol* **65.12** 125004.

[11] McCleskey M, Kaye W, Mackin D, Beddarc S, He Z and Polf J 2015 Evaluation of a multistage CdZnTe Compton camera for prompt gamma imaging for proton therapy *Nuclear Instruments and Methods in Physics Research Section A: Accelerators, Spectrometers, Detectors and Associated Equipment* **785** 163–169.

[12] Panthi R, Maggi P, Peterson S, Mackin M, Polf J and Beddar S 2020 Secondary particle interactions in a Compton camera designed for in vivo range verification of proton therapy *IEEE transactions on radiation and plasma medical sciences* **5.3** 383–391.

[13] Peterson S, Maggi P, Panthi R, Beddar S, Mackin D, and Polf J, 2020 Investigating the impact of secondaries neutrons on Compton camera for medical imaging [Poster].

[14] Tuckwell W and Bezak. E 2007 Calculation of the positron distribution from ^{15}O nuclei formed in nuclear reactions in human tissue during proton therapy *Phys. Med. Biol* **52.9** 2483.

[15] Jiang H, Wang B, Xu X, Suit H and Paganetti H 2005 Simulation of organ-specific patient effective dose due to secondary neutrons in proton radiation treatment *Phys. Med. Biol* **50.18** 4337.

[16] Streicher M, Goodman D, Zhu Y, Brown S and Kiff S 2017 Fast neutron detection using pixelated CdZnTe spectrometers *IEEE Transactions on Nuclear Science* **64.7** 1920–1926.

[17] Zhang F, He Z and Seifert C 2007 A prototype three-dimensional position sensitive CdZnTe detector array *IEEE Transactions on Nuclear Science* **54.4** 843–848.